J. Plasma Physics (2009), *vol.* 75, *part* 3, *pp.* 395–406. © 2009 Cambridge University Press
doi:10.1017/S0022377809007818 Printed in the United Kingdom

Collisional instability in a rare magnetized plasma: an experimental model for magnetospheric and space plasma study

CONSTANTINE L. XAPLANTERIS

Plasma Physics Lab, IMS, NCSR, 'Demokritos', Athens, Greece
(lfilip@ims.demokritos.gr)

(Received 6 August 2008, revised 12 October 2008 and accepted 28 November 2008, first published online 28 January 2009)

Abstract. In a suitable experimental device, laboratory plasma is produced with conditions and parameters analogous to magnetospheric plasma; we light a rare plasma in a semi-machine using rf-frequency discharge. Three ranges of low-frequency instabilities appear, one of which is identified as drift, caused by electron–neutral collisions. A full theoretical elaboration adapted to production conditions and geometrical symmetry is carried out; one solution of the dispersion relation is sufficient justification for the existence of the instability. The mathematical analysis also has the ambition to give interpretation for other low-frequency waves. Here we make a sound identification of the instability type as drift resistive due to electron–neutral collisions by an investigation of the growth rate. An agreement between experimental results and the theoretical model is obtained. As in the magnetosphere, an external magnetic field restrains the plasma.

1. Introduction

Drift waves have attracted much interest over recent decades. Drift instabilities are one of the major problems on the way towards an exploitable thermonuclear fusion, since they cause enhanced losses. Furthermore, drift waves appear in space plasma, as well as in the magnetosphere and magnetograph of the Earth (Silveira et al. 2002) and involve many other phenomena. Thus, the drift instabilities remain an open issue today, although they have been studied persistently.

The first experimental observations and measurements of the collisional drift instabilities were reported in the early 1960s (D'Angelo 1961; Chu et al. 1967; Hendel et al. 1967). A large contribution to the drift wave theory was also given by Chen the early 1960s (Chen 1965, 1967, 1979). Drift waves due to density, electric field and temperature gradients, in Q-machine plasmas, have been studied extensively in the years that followed (Ellis et al. 1980; Marden-Marshall et al. 1986). There is extensive literature on this subject (Wesson 1997) and a long list of references on previous works on the field could be constructed, but in the present paper we only mention a few of the most relevant works.

As drift waves are produced and propagate in the laboratory or space plasma, various phenomena are caused. Thus, they are affected by current-carrying dusty plasmas, where we have a coupling of drift waves with the dynamics of dust grains (Vranjes et al. 2004). Drift waves also trap plasma electrons, affecting plasma

https://doi.org/10.1017/S0022377809007818 Published online by Cambridge University Press

conductivity (Xaplanteris 1987). Moreover, since drift instabilities are controllable by external electrical signals, their study makes the understanding of wave–wave interaction feasible (Anastassiades and Xaplanteris 1983; Block et al. 2001).

Sometimes, we distinguish between the drift instabilities of the laboratory plasma instabilities (Anastassiades and Xaplanteris 1983; Benilov and Power 2007; Schröder et al. 2004, 2005; Shukla et al. 2002) and the magnetospheric and space plasma instabilities (Mikhailovskii et al. 2007; Silvers et al. 2002). However, this distinction is not clear today, as experiments are carried out using the simulation methods and the results can be valid for both laboratory and space plasmas (Vranjes and Poedts 2005; Vranjes et al. 2004; Salimullah et al. 2003, 2004).

Up to now drift waves have been the subject of investigation in various experiments and studied using different devices with various plasma parameter ranges, weakly ionized plasma as well as fully ionized plasma, magnetized and non-magnetized plasma, collisionless and collisional plasma. Most of the experiments have been carried out in plasmas with β (the ratio of plasma pressure to magnetic pressure) much smaller than the electron to ion mass ratio m_e/m_i. If β is small, drift waves are electrostatic, and in contrast, if β is larger, electromagnetic effects may become important and the wave becomes Alfvénic.

Schröder et al. (2004, 2005) defined a method of sound identification of a drift wave. Recently, Vranjes and Poedts (2007) have described the behavior of electrostatic drift and ion sound waves into plasmas, which have a density gradient that is perpendicular to and along the external magnetic field. In laboratory cylindrical plasmas, the parallel density gradient may be formed by the variation of the plasma density as we move away from the source. In a similar way, in space plasmas, as in the Solar coronal magnetic flux tubes, a parallel density gradient may be formed due to stratification in the external gravity field, or for other external reasons.

Plasma particle collisions give rise to diffusion and other transport processes. Thus, there is transfer of momentum and energy between particles resulting from plasma resistance. Collisions in plasmas depend on the particle relative velocities and the final result is the integrated effect of these interactions. The value of the electric field at a given point is the result of the distribution of all charged particles. Thus, each particle is subject to a force due to the electric field of all of the other particles and in the presence of a magnetic field we have a drift velocity (Wesson 1997).

Strong low-frequency waves appear almost persistently in our Q-machine quiescent plasma. In a previous paper (Anastassiades and Xaplanteris 1983) we presented the waves due to rf-frequency (rf)-field gradients and in here we study the effects of this instability on Hall plasma conductivity due to electron trapping.

In the present paper we present experimental results concerning drift waves due to the electron collisions with neutral atoms and molecules. Furthermore, we make an effort to understand the cause of these instabilities. A satisfactory interpretation based on a theoretical model is given.

In the present set-up, we increased the measuring capabilities concerning wave parameters and the plasma localization. All plasma parameters are taken close to magnetospheric plasma parameters, so that the experiment becomes a good simulation. The new instability is located in a cylindrical cell of average radius $R \cong 2.5$ cm, with standard spectrum and a frequency that is close to 100 kHz. As our theoretical model shows, electron–neutral collisions may cause growth. A good agreement between the experimental results and the mathematical approximation,

https://doi.org/10.1017/S0022377809007818 Published online by Cambridge University Press

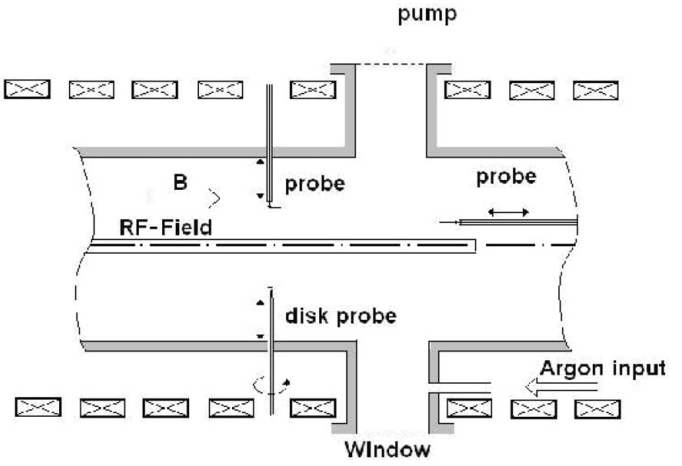

Figure 1. The experimental arrangement; the rf-field antenna, probes and disk probe are shown.

as well as some calculated values, can result in wave rotation around the system axis with phase velocity close to the electron drift u_e. In addition, the growth is caused by electron–neutral collisions ν_e, as the investigation of growth rate shows.

In Sec. 2 we give a description of our experimental device with its appropriate probes. A detailed account of the experimental observations, measurements and calculations is also given. An extensive study of the dispersion relation is presented in Sec. 3. In Sec. 4 we elaborate on the experimental results in relation to our theoretical model. Finally, in Appendix A the drift velocity for ions and electrons caused from any kind of electrical field gradient is determined. After this, in Appendix B the complete dispersion relation is found.

2. Experimental results

2.1. Description of the set-up

The experimental device is shown schematically in Fig. 1. A cylindrical metallic tube of a 6 cm inner diameter, approximately 70 cm length and with closed ends is placed into the magnetic field B, which is directed along the cylinder axis. A 5 mm-diameter and 40 cm length conductor is placed along the cylinder axis with one of its ends attached to the center of the cyclic base of the cylinder. This conductor together with the tube creates a coaxial conductive line through which the microwaves enter the cavity. An electrostatic cylindrical probe, which can be moved radially, has its metallic end oriented along the z-axis. The plasma density, the electron temperature and all of the wave parameters (e.g. frequencies, amplitudes, waveforms, spectrum) are measured with the help of this electrical probe (Wesson 1997). Another electrical probe is oriented along the magnetic field B and it can be moved parallel to the z-axis at a distance of 2 cm. Using this probe, the various parameters of the whole plasma column along the cylindrical cavity, can be determined. Moreover, we have placed a 2 mm diameter electrical probe, so that the drift currents can be measured. This disk probe can be moved radially as well as around its axis.

https://doi.org/10.1017/S0022377809007818 Published online by Cambridge University Press

Table 1. Average typical values of plasma parameters.

Parameters	Average typical values
Argon pressure p	0.40 Pa
Argon number density n_g	5.8×10^{19} m^{-3}
Magnetic field intensity B	80 mT
Microwaves' power P	70 W
Electron density n_0	5×10^{16} m^{-3}
Electron temperature T_e	2 eV
Ion temperature T_i	0.07 eV
Ionization rate	0.1%
Electron drift velocity u_e	1.2×10^4 m s^{-1}
Electron–neutral collision frequency v_e	2×10^7 s^{-1}

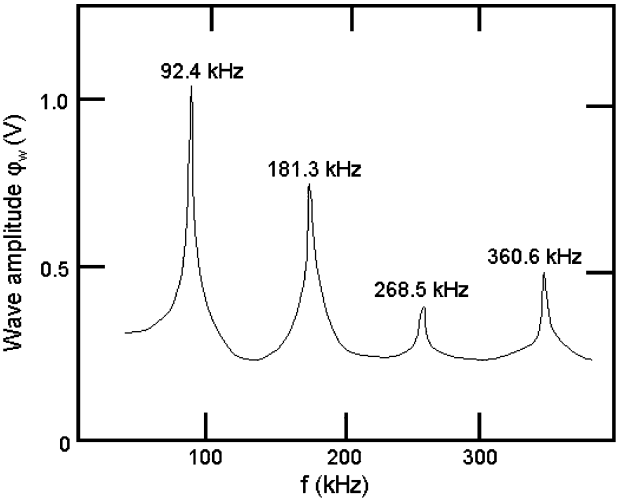

Figure 2. A typical wave spectrum with fundamental $f_1 \cong 92.4$ kHz and its higher harmonics.

Two portals have been fixed at the external cylinder side; the first is used to connect the cavity with the vacuum pump. The second portal is supplied with a glass window and the argon flows in through a side tube.

2.2. Experimental results

Our first concern was to determine the range of the magnetic field, rf-microwave power and pressure, keeping two of the parameters at typical values and varying the third. We found that plasma exists for magnetic fields in the range of 20–150 mT, rf-microwave power (input-reflected) of 35–150 W and pressure of 0.1–0.7 Pa. The plasma density varied in the range of 2×10^{16}–8×10^{16} m^{-3} and the electron temperature of 1.3–3.9 eV.

Average typical values of plasma parameters are listed in Table 1.

A typical wave spectrum is shown in Fig. 2. The parameter values are $W = 50$ W, $B = 40$ mT and $p = 0.11$ Pa. The fundamental frequency with its exact harmonics appears. It is easy to see that $f_l = l \cdot f_1$, $l = 1, 2, 3, \ldots$.

Figure 3(a) shows the plasma density radial profile, which presents the largest value at a distance $R \cong 2.0$ cm from the system axis. The density profile has the

https://doi.org/10.1017/S0022377809007818 Published online by Cambridge University Press

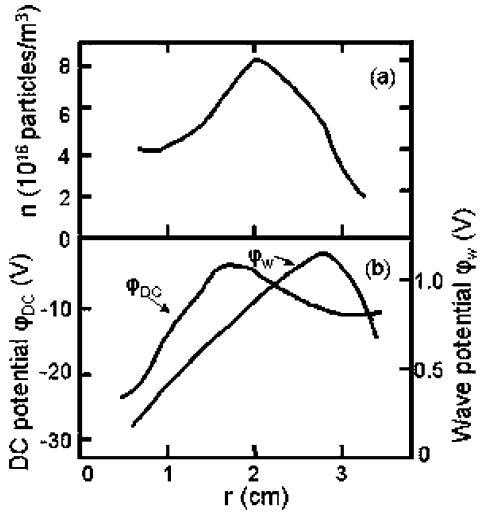

Figure 3. (a) A radial density profile. (b) The radial dc potential $\phi_{\rm dc}$ and the wave amplitude $\phi_{\rm W}$ are presented versus the distance r from the cylinder axis.

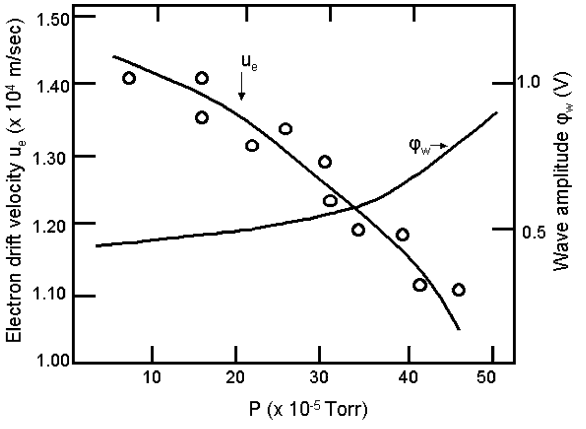

Figure 4. The electron drift velocity $u_{\rm e}$, the wave amplitude $\phi_{\rm W}$, and the wave frequency f, with points (○) in arbitrary units are plotted versus the pressure p. Electron drift measurements are taken with the disk probe placed at $R = 2.5$ cm, where the wave is strong. The accuracy is not high owing to the large dimensions of the probe.

same form as the rf power increases, although the absolute value grows linearly with the external microwave power. Typical radial profiles have been drawn in Fig. 3(b), for the dc potential $\phi_{\rm dc}$ and wave amplitude potential $\phi_{\rm W}$. The wave amplitude persists showing a maximum at a distance $R \cong 2.5$ cm from the axis, although the absolute value increases when the magnetic field B becomes smaller than $B_{\rm res}$.

Figure 4 shows the electron drift velocity versus the pressure; in the same diagram the wave amplitude and the wave frequency have been plotted. Measurements were taken with the disk probe, at $R = 2.5$ cm and for a magnetic field $B = 40$ mT. One can see that electron drift velocity and wave frequency decrease, whereas the wave amplitude grows as the pressure rises.

https://doi.org/10.1017/S0022377809007818 Published online by Cambridge University Press

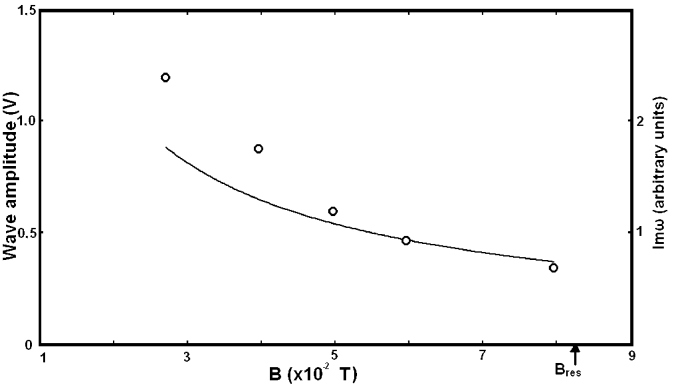

Figure 5. The amplitude of the wave potential is plotted versus the magnetic field B. The wave grows as the magnetic field deviates from $B_{\rm res}$. In addition, the theoretically calculated points ($\circ$) of the imaginary part $\omega_{\rm im}$ of the frequency are shown.

Finally, Fig. 5 presents the dependence of the wave amplitude on the magnetic field; measurements are taken at the usual distance from the axis for $p = 0.12$ Pa and $W = 45$ W. We see that the deviation from $B_{\rm res}$ causes a rapid increase of the wave amplitude.

3. Wave development ability

3.1. Case I

When the external magnetic field is equal to zero (no magnetized plasma and therefore $\omega_{\rm ci} = \omega_{\rm ce} = 0$), by using the complete dispersion relation (B 14) of Appendix B, we obtain the following relation

$$\left[\Pi_{\rm i}^2 - v_{\rm i}\Pi_{\rm i} + Q_{\rm i}^2\right] \cdot \left[\Pi_{\rm e}^2 - v_{\rm e}\Pi_{\rm e} + Q_{\rm e}^2\right] \cdot \Pi_{\rm i} \cdot \Pi_{\rm e} = \omega_{\rm pi}^2\omega_{\rm pe}^2 \cdot \Pi_{\rm i} \cdot \Pi_{\rm e}.$$

We consider the following particular cases.

- If $\Pi_{\rm i} = 0$, then $\omega = ku_{\rm i} - jv_{\rm i}$ and we have heavy damping when $ku_{\rm i} \leqslant v_{\rm i}$.
- If $\Pi_{\rm e} = 0$, then $\omega = ku_{\rm e} - jv_{\rm e}$ and very heavy damping occurs when $ku_{\rm e} \prec\prec v_{\rm e}$.
- If

$$\left[\Pi_{\rm i}^2 - \Pi_{\rm i}v_{\rm i} + \omega_{\rm pi}^2 + \Lambda_{\rm i}^2\right] \cdot \left[\Pi_{\rm e}^2 - \Pi_{\rm e}v_{\rm e} + \omega_{\rm pe}^2 + \Lambda_{\rm e}^2\right] = \omega_{\rm pi}^2 \cdot \omega_{\rm pe}^2 \qquad (1)$$

and there are no drift velocities, that is, when $u_{\rm i} = u_{\rm e} = 0$ it follows that $\Pi_k = v_k - j\omega$, where $k = {\rm e}, {\rm i}$. Then, relation (1) gives the two branches of acoustic modes, the ion-acoustic wave (low-frequency mode) and the electron-acoustic wave (high-frequency mode).

3.2. Case II

Next we consider the case $\omega_{\rm ci}, \omega_{\rm ce} \neq 0$.

For the low-frequency limit, $\omega \prec\prec v_{\rm e}, \omega_{\rm pi}$ and $\omega_{\rm pi}^2 \succ\succ \omega_{\rm ci}^2, k^2U_{\rm i}^2$, we have $Q_{\rm i}^2 \succ\succ \omega_{\rm ci}^2$ and the dispersion relation (B.14) becomes:

$$\Pi_{\rm e}^3 - v_{\rm e}\Pi_{\rm e}^2 + Q_{\rm e}^2\Pi_{\rm e} - v_{\rm e}\omega_{\rm ce}^2 = \frac{\omega_{\rm pi}^2\omega_{\rm pe}^2\Pi_{\rm e}}{\Pi_{\rm i}^2 - v_{\rm i}\Pi_{\rm i} + Q_{\rm i}^2},$$

https://doi.org/10.1017/S0022377809007818 Published online by Cambridge University Press

from which we have

$$\left\{\Pi_e^2+\omega_{ce}^2+k^2U_e^2+\omega_{pe}^2\left(1-\frac{\omega_{pi}^2}{\Pi_i^2-v_i\Pi_i+Q_i^2}\right)\right\}\cdot(\Pi_e-v_e)$$

$$=-\left\{k^2U_e^2+\omega_{pe}^2\left(1-\frac{\omega_{pi}^2}{\Pi_i^2-v_i\Pi_i+Q_i^2}\right)\right\}\cdot v_e. \tag{2}$$

After using the relation $\Pi_i^2-v_i\Pi_i=-(ku_i-\omega)^2+jv_i(ku_i-\omega)$ proved in Appendix B, relation (2) becomes

$$\left[\omega_{ce}^2+j\frac{v_i(ku_i-\omega)\omega_{pe}^2}{\omega_{pi}^2}\right]j(ku_i-\omega)$$

$$=-\left[k^2U_e^2+\frac{\omega_{pe}^2}{\omega_{pi}^2}\left(\omega_{ci}^2+k^2U_i^2-(ku_i-\omega)^2\right)+j\frac{\omega_{pe}^2}{\omega_{pi}^2}v_i(ku_i-\omega)\right]\cdot v_e.$$

Considering $\omega\cong ku_e$, we finally find

$$\omega\cong ku_e+jv_e\left[\frac{k^2(u_i-u_e)^2-\omega_{ci}^2-k^2U_i^2}{\omega_{ce}^2}\cdot\frac{\omega_{pe}^2}{\omega_{pi}^2}-\frac{k^2U_e^2}{\omega_{ce}^2}\right]. \tag{3}$$

Using the relation

$$k^2U_e^2\cdot\frac{\omega_{pi}^2}{\omega_{pe}^2}=k^2\frac{k_BT_e}{m_i}=k^2\cdot C_s^2,$$

then the relation (3) becomes

$$\omega\cong ku_e+jv_e\frac{\omega_{pe}^2}{\omega_{pi}^2}\frac{k^2(u_i-u_e)^2-k^2(U_i^2+C_s^2)-\omega_{ci}^2}{\omega_{ce}^2}. \tag{4}$$

Since $T_e\succ\succ T_i$, we have $C_s^2\succ\succ U_i^2$ and (4) can be written as

$$\omega\cong ku_e+jv_e\frac{\omega_{pe}^2}{\omega_{pi}^2}\cdot\frac{k^2(u^2-C_s^2)-\omega_{ci}^2}{\omega_{ce}^2}, \tag{5}$$

where $u=|u_i-u_e|$ is the relative drift velocity between electrons and ions.

Equation (5) can give growth under the conditions of our experiment as explained in Sec. 4. Evidently growth requires a strong drift, that is,

$$k^2u^2\succ k^2C_s^2+\omega_{ci}^2.$$

We next elaborate more on (3).

When

$$k^2u^2\succ k^2\left(U_i^2+C_s^2\right)+\omega_{ci}^2\succ k^2C_s^2, \tag{6}$$

that is, $u=|u_e-u_i|\succ C_s$, the other two low-frequency solutions can be obtained when (B.14) takes the form

$$\left[\Pi_e^2-v_e\Pi_e+\left(Q_e^2-\frac{\omega_{pi}^2\omega_{pe}^2}{\Pi_i^2-v_i\Pi_i+Q_i^2}\right)\right]\cdot\Pi_e=v_e\cdot\omega_{ce}^2. \tag{7}$$

For the low-frequency limit the inequality $\omega, ku_e\prec\prec v_e$ is valid and $\Pi_e\cong v_e$ for the multiplier Π_e in the parentheses.

https://doi.org/10.1017/S0022377809007818 Published online by Cambridge University Press

In addition,

$$\Pi_{\mathrm{i}}^2 - v_{\mathrm{i}}\Pi_{\mathrm{i}} = -(ku_{\mathrm{i}} - \omega)^2 + jv_{\mathrm{i}}(ku_{\mathrm{i}} - \omega)$$

$$\Pi_{\mathrm{e}}^2 - v_{\mathrm{e}}\Pi_{\mathrm{e}} = -(ku_{\mathrm{e}} - \omega)^2 + jv_{\mathrm{e}}(ku_{\mathrm{e}} - \omega)$$

and (7) becomes

$$\begin{aligned}\left[Q_{\mathrm{i}}^2 - (ku_{\mathrm{i}} - \omega)^2\right] \cdot \left[\omega_{\mathrm{pe}}^2 + k^2U_{\mathrm{e}}^2 - (ku_{\mathrm{e}} - \omega)^2\right] + jv_{\mathrm{i}}(ku_{\mathrm{i}} - \omega) \\ \cdot \left[\omega_{\mathrm{pe}}^2 + k^2U_{\mathrm{e}}^2 - (ku_{\mathrm{e}} - \omega)^2\right] - \omega_{\mathrm{pi}}^2\omega_{\mathrm{pe}}^2 + jv_{\mathrm{e}}(ku_{\mathrm{e}} - \omega) \\ \cdot \left[Q_{\mathrm{i}}^2 - (ku_{\mathrm{i}} - \omega)^2\right] + j^2v_{\mathrm{i}}v_{\mathrm{e}}(ku_{\mathrm{e}} - \omega) \cdot (ku_{\mathrm{e}} - \omega) = 0. \end{aligned} \tag{8}$$

Neglecting the collision terms and considering that $\omega_{\mathrm{pe}}^2 \succ\succ k^2U_{\mathrm{e}}^2, (ku_{\mathrm{e}} - \omega)^2$, then (8) takes the form

$$Q_{\mathrm{i}}^2 - (ku_{\mathrm{i}} - \omega)^2 \cong \frac{\omega_{\mathrm{pi}}^2\omega_{\mathrm{pe}}^2}{\omega_{\mathrm{pe}}^2 + k^2U_{\mathrm{e}}^2}. \tag{9}$$

We also have

$$\frac{\omega_{\mathrm{pi}}^2\omega_{\mathrm{pe}}^2}{\omega_{\mathrm{pe}}^2 + k^2U_{\mathrm{e}}^2} \cong \omega_{\mathrm{pi}}^2\left(1 - \frac{k^2U_{\mathrm{e}}^2}{\omega_{\mathrm{pe}}^2}\right) = \omega_{\mathrm{pi}}^2 - k^2C_{\mathrm{s}}^2$$

and then (9) gives

$$\omega \cong ku_{\mathrm{i}} \pm \sqrt{k^2U_{\mathrm{i}}^2 + k^2C_{\mathrm{s}}^2 + \omega_{\mathrm{ci}}^2}. \tag{10}$$

If $kC_{\mathrm{s}} \succ\succ kU_{\mathrm{i}}, \omega_{\mathrm{ci}}$, the last equation is simplified as follows:

$$\omega \cong k(u_{\mathrm{i}} + C_{\mathrm{s}}) - j\frac{v_{\mathrm{i}}}{2} + j\frac{m_{\mathrm{e}}}{m_{\mathrm{i}}}\frac{v_{\mathrm{e}}}{2}\frac{u_{\mathrm{e}} - (u_{\mathrm{i}} + C_{\mathrm{s}})}{C_{\mathrm{s}}} \tag{11}$$

or

$$\omega \cong k(u_{\mathrm{i}} - C_{\mathrm{s}}) - j\frac{v_{\mathrm{i}}}{2} - j\frac{m_{\mathrm{e}}}{m_{\mathrm{i}}}\frac{v_{\mathrm{e}}}{2}\frac{u_{\mathrm{e}} - (u_{\mathrm{i}} - C_{\mathrm{s}})}{C_{\mathrm{s}}}.$$

The last two equations clearly lead to the conclusion that we can have growth rate of resistive instabilities under the conditions stated above.

4. Interpretation of the results

In Fig. 2 we show the wave spectrum with its fundamental frequency $f_1 \cong 92.4$ kHz and its exact upper harmonics. This is in accordance with (5), where $\omega \cong ku_{\mathrm{e}} = (l/R)\Omega_{\mathrm{e}} \cdot R = l \cdot \Omega_{\mathrm{e}}$, $l = 1, 2, 3, \ldots$, $\Omega_{\mathrm{e}} = u_{\mathrm{e}}/R$ is the electron drift angular velocity. From Fig. 2 (and Fig. 4 below), we confirm that the maximum wave frequency $f_{1,\max} \cong 92.4$ kHz occurs at the maximum electron drift velocity $u_{\mathrm{e}} = 1.45 \times 10^4$ m s^{-1}, while the minimum wave frequency $f_{1,\min} \cong 70$ kHz occurs at the minimum drift value $u_{\mathrm{e}} \cong 1.10 \times 10^4$ m s^{-1}.

After observing the wave, we had to measure certain properties of the plasma necessary for the calculation of its parameters. In Fig. 3(a) the density profile is depicted, while in Fig. 3(b) the dc and wave amplitude potentials are given and, from their gradients, the drift velocities have been located.

In Fig. 4 the small circles (○) show the wave frequency f (arbitrary units) versus pressure. The linear relation between wave frequency and electron drift velocity is

https://doi.org/10.1017/S0022377809007818 Published online by Cambridge University Press

Table 2. Imaginary parts of ω and wave amplitudes versus the magnetic field B. For calculating E_0'/E_0 we used the relation $E_0'/E_0 \propto e^{(\omega_{\rm im}/\omega)\times 100}$.

$B(\times 10^{-2}$ T)	$\omega_{\rm im}(\times 10^5$ rad s$^{-1})$	$(\omega_{\rm im}/\omega)\times 100$	$(E_0'/E_0) \propto e^{(\omega_{\rm im}/\omega)} \times 100$
8	0.094	1.6	1.016
6	0.166	2.9	1.029
5	0.24	4.13	1.042
4	0.374	6.45	1.067
3	0.665	11.48	1.122

easily confirmed. The electron drift velocity is reduced as the pressure increases because of the fact that the electron–neutral collisions are opposed to the electron drift motion.

We next examine the ability of growth rate: the imaginary part of the wave frequency is

$$\omega_{\rm im} = v_{\rm e} \cdot \frac{\omega_{\rm pe}^2}{\omega_{\rm pi}^2} \cdot \frac{(ku)^2}{\omega_{\rm ce}^2} \Rightarrow \omega_{\rm im} = v_{\rm e} \cdot \frac{m_{\rm e} \cdot m_{\rm i} \cdot (ku)^2}{e^2} \cdot \frac{1}{B^2} \tag{12}$$

and the electron collision time $\tau_{\rm e}$ in our experiment is estimated to be very small ($\tau_{\rm e} \prec 0.0132\ \mu$s), due to the low electron temperature $T_{\rm e}$ (Wesson 1997). Therefore, the electron collision frequency $v_{\rm e}$ always exceeds 7.6×10^7 Hz, and, under our experimental conditions, it may give the growth rate. This is in agreement with Fig. 4, where the wave amplitude increases as the pressure p assumes larger values.

Another experimental result concerns the influence of the magnetic field B on the wave amplitude. In Fig. 5 one can observe the decrease of the growth rate as the magnetic field becomes stronger, in agreement with (12), which assumes the numerical form

$$\omega_{\rm im} \cong 15.5x \frac{1}{B^2} \quad B \text{ in } T(\text{Weber/m}^2).$$

For the physical explanation we must consider two opposite views. The first is that as the magnetic field increases while approaching $B_{\rm res}$, the plasma density also increases, and $v_{\rm e}$ becomes larger. According to the other view, when the magnetic field increases, the motion of electrons is limited and consequently $v_{\rm e}$ decreases. In the present case, the second view appears to be the predominant one.

Table 2 shows the calculated results for $\omega_{\rm im}$ and the growth for certain values of the magnetic field. As one can see from Figure 5, the calculated points of $\omega_{\rm im}$ versus B, ($\circ$), are in good agreement with the wave amplitude measurements.

One can conclude that our experimental results (Table 2 and Figs 2–5) are in agreement with the dispersion relation (5). In addition, the waves caused by electron–neutral collisions are interpreted as of 'resistive instability' type.

Acknowledgements

The author wishes to thank Dr A. J. Anastassiades for his valuable help in theoretical as well as experimental subjects. He is also grateful to Dr Y. Bassiakos, Dr E. Filippaki and other members of Plasma Laboratory of NCSR, 'Demokritos' for their assistance in various ways.

https://doi.org/10.1017/S0022377809007818 Published online by Cambridge University Press

Appendix A. Drift velocities

Using $\mathbf{u}$ to denote the total drift velocity due to the electric field ε and $\upsilon(\mathbf{r},t)$ to denote the perturbed velocities caused by the plasma electric field wave $\mathbf{E}(\mathbf{r},t)$, the whole magnitude can be written as $\mathbf{V}=\mathbf{u}+\upsilon(\mathbf{r},t)$.

We make the hypothesis that all perturbed magnitudes are harmonic, that is,

$$\mathbf{E}(\mathbf{r},t)=\hat{e}_x\cdot E\cdot e^{j(kx-\omega t)}$$

$$\upsilon(\mathbf{r},t)=\upsilon\cdot e^{j(kx-\omega t)}$$

$$p\propto e^{j(kx-\omega t)}\quad\text{(pressure)}$$

$$n(\mathbf{r},t)=n\cdot e^{j(kx-\omega t)}\quad\text{(density)}.$$

Then, for $\mathbf{B}=\hat{e}_z\cdot B$, the following relations are valid:

$$\varepsilon=\hat{e}_y\cdot\varepsilon,\mathbf{u}=\hat{e}_x\cdot u$$

and the total density is $N(\mathbf{r},t)=n_0+n(\mathbf{r},t)$.

The momentum equation for both kinds of charged particle (ions and electrons) is

$$Nm\left[\frac{\partial}{\partial t}+\mathbf{V}\cdot\nabla\right]\cdot\mathbf{V}=N\cdot q(\mathbf{E}+\varepsilon)+N\cdot q\cdot\frac{\mathbf{V}\times\mathbf{B}}{c}-Nmv\mathbf{V}-\nabla p. \tag{A 1}$$

When there are no waves, $\mathbf{E},\mathbf{u}(\mathbf{r},t)$ and n vanish and (A 1) becomes

$$\mathbf{0}=n_0q\varepsilon+n_0q\frac{\mathbf{u}\times\mathbf{B}}{c}-n_0mv\mathbf{u} \tag{A 2}$$

and the drift velocity u, with $q=\mathrm{e}$ for ions and $q=-\mathrm{e}$ for electrons can be determined.

Using cylindrical coordinates θ and r, we find the corresponding drift velocities:

$$u_\theta=\frac{q\varepsilon}{m}\cdot\frac{\omega_\mathrm{c}}{\omega_\mathrm{c}^2+v^2}\quad\text{and}\quad u_r=\frac{v}{\omega_\mathrm{c}}\cdot u_\theta.$$

When the ion–neutral collisions are negligible, $v=0$ and the last equations give

$$u_\theta=\frac{\varepsilon}{B}\quad\text{and}\quad u_r=0.$$

Appendix B. Dispersion relation

Equations (A 1) and (A 2) give the momentum equation:

$$nm\left(\frac{\partial}{\partial t}+u\cdot\nabla\right)\vec{v}=nq\left(\mathbf{E}+\frac{\upsilon\times\mathbf{B}}{c}\right)-\nabla p-nmv\upsilon. \tag{B 1}$$

The continuity equation assumes the form

$$\frac{\partial n}{\partial t}+\mathbf{u}\cdot\nabla n+n_0\cdot\nabla\upsilon=0. \tag{B 2}$$

Using the indices x and y for the vector components corresponding to r and θ of our cylindrical system and taking $U^2\equiv k_\mathrm{B}T/m$ and $\Pi\equiv j(ku-\omega)+v$, the

https://doi.org/10.1017/S0022377809007818 Published online by Cambridge University Press

momentum equation (B 1) becomes

$$\Pi v_x - \omega_c v_y = -j\frac{q}{m}k\phi - jkU^2\frac{n}{n_0}, \tag{B 3}$$

$$\Pi v_y + \omega_c v_x = 0. \tag{B 4}$$

From Poisson's equation

$$\nabla^2 \cdot \phi = 4\pi \cdot e(n_e - n_i) \tag{B 5}$$

we have

$$k^2\phi = 4\pi \cdot e(n_i - n_e) \tag{B 6}$$

and the continuity equation becomes:

$$-\omega n + knu + n_0 k v_x = 0 \tag{B 7}$$

or

$$v_x = j\frac{\Pi - v}{k} \cdot \frac{n}{n_0}. \tag{B 8}$$

From (B 3), (B 4), (B 6) and (B 8) with $\Lambda^2 \equiv k^2U^2$, after some mathematical elaboration we obtain

$$\left[\Pi(\Pi - v) + \omega_c^2\frac{\Pi - v}{\Pi} + \Lambda^2\right] \cdot n = \frac{q}{|q|}\omega_p^2(n_e - n_i), \tag{B 9}$$

where $\omega_p^2 = 4\pi e^2 n_0/m$ is the plasma frequency.

Equation (B 9) for ions has the form

$$\left[\Pi_i(\Pi_i - v_i) + \omega_{ci}^2\frac{\Pi_i - v_i}{\Pi_i} + \Lambda_i^2 + \omega_{pe}^2\right] \cdot n_i = \omega_{pi}^2 n_e \tag{B 10}$$

and for electrons it has the form

$$\left[\Pi_e(\Pi_e - v_e) + \omega_{ce}^2\frac{\Pi_e - v_e}{\Pi_e} + \Lambda_e^2 + \omega_{pe}^2\right] \cdot n_e = \omega_{pe}^2 \cdot n_i^2. \tag{B 11}$$

By introducing the notation

$$\omega_{ci}^2 + \omega_{pi}^2 + \Lambda_i^2 \equiv Q_i^2, \quad \omega_{ce}^2 + \omega_{pe}^2 + \Lambda_e^2 \equiv Q_e^2,$$

the last two equations become

$$\left[\Pi_i(\Pi_i - v_i) - \omega_{ci}^2\frac{v_i}{\Pi_i} + Q_i^2\right] \cdot n_i = \omega_{pi}^2 \cdot n_e, \tag{B 12}$$

$$\left[\Pi_e(\Pi_e - v_e) - \omega_{ce}^2\frac{v_e}{\Pi_e} + Q_e^2\right] \cdot n_e = \omega_{pe}^2 \cdot n_i. \tag{B 13}$$

Finally, after multiplication by parts we have

$$\left[\Pi_i^3 - v_i\Pi_i^2 - v_i\omega_{ci}^2 + Q_i^2\Pi_i\right] \cdot \left[\Pi_e^3 - v_e\Pi_e^2 - v_e\omega_{ce}^2 + Q_e^2\Pi_e\right] = \omega_{pi}^2\omega_{pe}^2\Pi_i\Pi_e, \tag{B 14}$$

which is the complete dispersion relation, when a plasma with streaming particles exists perpendicular to the magnetic field.

https://doi.org/10.1017/S0022377809007818 Published online by Cambridge University Press

References

Anastassiades, A. and Xaplanteris, C. 1983 *J. Phys. Soc. Jpn* **52**, 492.
Benilov, S. E. and Power, A. O. 2007 *Phys. Plasmas* **14**, 082101.
Block, D., Piel, A. Schröder, Ch. and Klinger, T. 2001 *Phys. Rev.* E **63**, 056401.
Chen, F. F. 1965 *Phys. Fluids* **8**, 1323.
Chen, F. F. 1967 *Phys. Fluids* **10**, 1647.
Chen, F. F. 1979 *Phys. Fluids* **22**, 2346.
Chu, K. T., Hendel, W. H. and Politzer, A. P. 1967 *Phys. Rev. Lett.* **19**, 1110.
D'Angelo, N. 1961 *Phys. Fluids* **4**, 1054.
Ellis, F. R., Marden-Marshall, E. and Majeski, R. 1980 *Plasma Phys.* **22**, 113.
Hendel, W. H., Coppi, B., Perkins, F. and Politzer, A. P. 1967 *Phys. Rev. Lett.* **18**, 439.
Marden-Marshall, E., Ellis, F. R. and Walsh E. J. 1986 *Plasma Phys.* **28**, No 9B.
Mikhailovskii, B. A. et al. 2007 *Phys. Plasmas* **14**, 112108.
Salimullah, M., Rizwan, M. A., Nambu, M. and Shukla, K. P. 2004 *Phys. Rev.* E **70**, 026404.
Salimullah, M., Sandberg, I. and Shukla, K. P. 2003 *Phys. Rev.* E **68**, 027403.
Schröder, C., Grulke, O., Klinger, T. and Naulin, V. 2004 *Phys. Plasmas* **11**, 4249.
Schröder, C., Grulke, O., Klinger, T. and Naulin, V. 2005 *Phys. Plasmas* **12**, 042103.
Shukla, K. P., Sorasio, G. and Stenflo, L. 2002 *Phys. Rev.* E **66**, 067401.
Silveira, J. O., Ziebell, F. L., Gaeizer, R. and Yoon, H. P. 2002 *Phys. Rev.* E **65**, 036407.
Vranjes, J. and Poedts, S. 2005 *Phys. Plasmas* **12**, 064501.
Vranjes, J. and Poedts, S. 2007 *Phys. Plasmas* **14**, 112106.
Vranjes, J., Sallem, I. and Poedts, S. 2004 *Phys. Rev.* E **69**, 056404.
Wesson, J., 1997 *Tokamaks*, 2nd edn. Oxford: Clarendon Press, pp. 51, 394.
Xaplanteris, L. C. 1987 *Astrophys. Space Sci.* **136**, 171.

https://doi.org/10.1017/S0022377809007818 Published online by Cambridge University Press